Cerebral Cortex, January 2021;31: 48–61

doi: 10.1093/cercor/bhaa203
Advance Access Publication Date: 21 September 2020
Original Article

ORIGINAL ARTICLE

Sulcal Depth in the Medial Ventral Temporal Cortex Predicts the Location of a Place-Selective Region in Macaques, Children, and Adults

Vaidehi S. Natu[1], Michael J. Arcaro[2,3], Michael A. Barnett[3], Jesse Gomez[4,5], Margaret Livingstone[2], Kalanit Grill-Spector[1,6,7] and Kevin S. Weiner[4,5]

[1]Department of Psychology, Stanford University, Stanford, CA 94305, USA, [2]Department of Neurobiology, Harvard Medical School, MA 02115, USA, [3]Department of Psychology, University of Pennsylvania, Philadelphia, PA 19104, USA, [4]Department of Psychology, University of California, Berkeley, CA 94720, USA, [5]Helen Wills Neuroscience Institute, University of California, Berkeley, Berkeley, CA 94720, USA, [6]Neurosciences Program, Stanford University, Stanford, CA 94305, USA and [7]Wu Tsai Neurosciences Institute, Stanford University, Stanford, CA 94305, USA

Address correspondence to Vaidehi S. Natu, Department of Psychology, Stanford University, Stanford, CA 94305, USA. Email: vnatu@stanford.edu.

Abstract

The evolution and development of anatomical–functional relationships in the cerebral cortex is of major interest in neuroscience. Here, we leveraged the fact that a functional region selective for visual scenes is located within a sulcus in the medial ventral temporal cortex (VTC) in both humans and macaques to examine the relationship between sulcal depth and place selectivity in the medial VTC across species and age groups. To do so, we acquired anatomical and functional magnetic resonance imaging scans in 9 macaques, 26 human children, and 28 human adults. Our results revealed a strong structural–functional coupling between sulcal depth and place selectivity across age groups and species in which selectivity was strongest near the deepest sulcal point (the sulcal pit). Interestingly, this coupling between sulcal depth and place selectivity strengthens from childhood to adulthood in humans. Morphological analyses suggest that the stabilization of sulcal–functional coupling in adulthood may be due to sulcal deepening and areal expansion with age as well as developmental differences in cortical curvature at the pial, but not the white matter surfaces. Our results implicate sulcal features as functional landmarks in high-level visual cortex and highlight that sulcal–functional relationships in the medial VTC are preserved between macaques and humans despite differences in cortical folding.

Key words: functional magnetic resonance imaging (fMRI), human development, macaque, sulcal depth, sulcal pits

Introduction

The primate visual cortex comprises a few dozen visual areas spanning occipital, temporal, and parietal cortices (Felleman and Van Essen 1991; Van Essen et al. 2001; Rosa and Tweedale 2005). Although the topological layout of these areas is similar across individuals within a particular species (Dumoulin et al. 2000; Tsao et al. 2003; Larsson and Heeger 2006; Grill-Spector and Weiner 2014; Kolster et al. 2014; Witthoft et al. 2014; Arcaro and Kastner 2015; Arcaro and Livingstone 2017), the shape and size of brains vary considerably across species (Sereno and Tootell 2005; Zilles et al. 2013). Despite this variability, there is a strong correspondence between sulcal folding and the functional organization of the primary visual cortex (V1). In both humans and monkeys, V1 is localized to the calcarine sulcus (Tootell et al. 1998; Hinds et al. 2008; Rajimehr and Tootell 2009; Benson et al. 2012), and surface topology is predictive of the underlying

retinotopic representations (Rajimehr and Tootell 2009; Benson et al. 2012). Beyond V1, the traditional view is that there is little correspondence between sulcal folding and visual areas given that 1) there are more brain areas than there are sulci, 2) the number of sulci varies across primates, and 3) there is a relatively large degree of individual variability in the size and topological layout of the cortex beyond primary sensory areas (Zilles et al. 2013; Van Essen et al. 2019).

Nevertheless, the last decade has shown renewed interest in the relationship between sulcal folding and functional regions (Benson et al., 2012, 2014; Amiez and Petrides 2014; Weiner et al. 2014; Witthoft et al. 2014; Leroy et al. 2015; Amiez et al. 2018, 2019; Bodin et al. 2018; Lopez-Persem et al. 2019; Weiner 2019). There is a surprising level of orderliness between sulcal folds and functional representations in even the higher-level processing stages of the visual hierarchy in humans (children and adults; Weiner and Grill-Spector 2010, 2011; Grill-Spector and Weiner 2014; Weiner et al. 2018), as well as macaques (Nasr et al. 2011; Arcaro and Livingstone 2017). Furthermore, focusing on sulcal landmarks as predictors of human high-level visual regions has revealed a coupling between sulcal features (as opposed to entire sulci) and functional regions. For example, in human VTC, there is a strong predictable relationship between 1) the anterior tip of the mid-fusiform sulcus and the location of a functional region selective to faces (Weiner et al. 2014) and 2) a sulcal intersection in the medial VTC and the location of a region selective for visual places and scenes (Weiner et al. 2018).

Beyond large-scale sulcal folding patterns, there is also interest in morphological features of sulci including sulcal depth and the physical location along the sulcal fold with the deepest depth, which is known as the sulcal pit (Regis et al. 2005; Leroy et al. 2015; Auzias et al. 2015; Im and Grant 2019). The sulcal pit is interesting because it is hypothesized to be associated with functional specialization (Rakic 1988; Welker 1990; Regis et al. 2005; Hasnain et al. 2006; Lohmann et al. 2008; Im et al. 2010, 2011; Im and Grant 2019; Meng et al. 2014; Auzias et al. 2015; Leroy et al. 2015; Bodin et al. 2018). In adult humans, sulcal pits are shown to predict cognitive skills such as verbal IQ (Im et al. 2011), as well as the location of functional regions selective for human voices and social communication (Bodin et al. 2018). These previous studies highlight that the predictive value of the sulcal pit comes from the actual depth measurement as opposed to other properties of the sulcus at the deepest point (e.g., mean curvature, laminar composition, cortical thickness, etc.). Additionally, a stable spatial distribution of sulcal pits also exists at birth with regionally heterogeneous growth patterns in sulcal depth over the first 2 years of infant life (Meng et al. 2014). Thus, growing evidence suggests that morphology of sulcal folds, specifically sulcal pits, may have a tight coupling with functional regions—even in association cortices. Nevertheless, the relationship between sulcal depth and functional selectivity across development and species remains untested.

Here, we leveraged the anatomical–functional relationship between sulci in the medial VTC and place selectivity to examine the relationship between sulcal depth and functional selectivity across development and species. This place-selective region in the medial VTC is interesting to study from a developmental perspective because it 1) emerges within 6 months postnatally in humans (Deen et al. 2017); 2) it appears to be functionally mature in early childhood (Golarai et al. 2007, 2010; Scherf et al. 2007; Gomez et al. 2017), while also exhibiting prolonged morphological development during childhood (Natu et al. 2019); and 3) there is a proposed homologous place-selective region in the medial VTC of macaques (Kornblith et al. 2013; Arcaro and Livingstone 2017). To explore the relationship between place selectivity and sulcal morphology, we asked two main questions: 1) Is there a consistent anatomical–functional relationship between sulcal depth and the location of a place-selective region in the human medial VTC? 2) Does this relationship change across developmental (childhood to adulthood) or evolutionary timescales? To answer these questions, we acquired anatomical and functional magnetic resonance imaging (fMRI) scans in adult rhesus macaques, as well as human children and adults.

Materials and Methods

Participants

Humans

Twenty-six children (ages 5–12 years, 17 females) and 28 adults (ages 22–28 years, 14 females) participated in our study. Children were recruited from the Palo Alto public school district through flyers and online advertisements. Adult participants are Stanford University affiliates. MRI data were collected using a 3 T GE scanner in the Center for Cognitive and Neurobiological Imaging at Stanford University. All participants had normal or corrected-to-normal vision and provided written, informed consent. Protocols were approved by the Stanford Internal Review Board on Human Participants.

Macaques

Nine rhesus macaques (ages 1–5 years, 4 females) participated in our study. One year in rhesus macaque age is thought to correspond to approximately 4 years in human age. All procedures were approved by the Harvard Medical School Animal Care and Use Committee and conformed to the National Institute of Health guidelines for the humane care and use of laboratory animals. Anatomical MRI data were collected using a 3 T Siemens Skyra scanned in Brigham and Women's hospital. Functional MRI data were collected using a 3 T TimTrio scanner in the Athinoula A. Martinos Center for Biomedical Imaging of Massachusetts General Hospital.

Data Acquisition in Humans (Anatomical Scans)

For human subjects, participants were scanned using spin-echo inversion recovery with an echo-planar imaging (EPI), readout (SEIR-EPI), with a 3 T GE Signa scanner and a custom-built, phase array 32-channel, receive-only, head coil using methods as in prior studies (Mezer et al. 2013; Natu et al. 2016, 2019; Gomez et al. 2017, 2018; Nordt et al. 2018). This scan was done with a slab inversion pulse and spatial–spectral fat suppression. We used a 2 mm^2 in-plane resolution with a slice thickness of 4 mm, and the EPI readout was performed using 2× acceleration. QMRI parameters were measured from spoiled gradient echo images acquired with different flip angles ($\alpha = 4°$, 10°, 20°, and 30°, TR = 14 ms, TE = 2.4 ms) and a voxel resolution of $0.8 \times 0.8 \times 1$ mm, which was resampled to 1 mm^3 isotropic. For SEIR-EPI, the TR was 3 s. The echo time was set to minimum full; inversion times were 50, 400, 1200, and 2400 ms. Anatomical data were aligned to the AC–PC plane. From the qMRI data, we generated the whole-brain T_1-weighted anatomy. The spoiled GE and the SEIR scans were processed using the mrQ software package in MATLAB to produce the T_1 maps. The mrQ analysis pipeline corrects for RF coil bias using SEIR-EPI scans, producing

accurate T_1 fits across the brain. The full analysis pipeline can be found at https://github.com/mezera/mrQ (Mezer et al. 2013).

Reconstruction of Cortical Surfaces

Human T_1 images underwent automated cortical surface reconstruction using FreeSurfer's auto-segmentation software (http://freesurfer.net). The anatomical images were segmented into white and gray matter. White matter surfaces were inspected and manually fixed for missing or mislabeled white matter voxels using ITK-SNAP (http://www.itksnap.org/). A mesh of each participant's cortical surface was generated from the boundary of the white and gray matter, and this mesh was inflated for visualization of functional activations inside the sulci.

Functional Scans

Functional data were obtained with the same scanner and coil using a T2*-sensitive gradient echo spiral pulse sequence with a resolution of $2.4 \times 2.4 \times 2.4$ mm, TR = 1000 ms, TE = 30 ms, flip angle = 76°, and FOV = 192 mm. We collected 48 oblique slices, oriented parallel to the superior temporal sulcus as in our previous work (Stigliani et al. 2015; Natu et al. 2016, 2019; Gomez et al. 2017, 2018; Nordt et al. 2018; Weiner et al. 2018), using a multiplexing, multi-slice technique (3 slabs of 16 slices; Feinberg et al. 2010), which enabled the whole-brain coverage of functional data. During MRI scanning, participants were lying supine inside the magnet. Visual stimuli were projected onto a monitor and were viewed through an angled mirror mounted above the participant's head. We defined place-selective regions of interest (ROIs) in individual participants using a functional localizer experiment based on our prior methods (Stigliani et al. 2015; Natu et al. 2016, 2019; Gomez et al. 2017, 2018; Nordt et al. 2018; Weiner et al. 2018). Participants completed 3 runs of a functional localizer experiment (5.24 min/run) with 78, 4 s blocks in each run. Participants viewed gray-scale stimuli, which were blocked by category. Images consisted of two subtypes from each of the five categories: places (houses and indoor scenes), human faces (child faces and adult faces), characters (numbers and pseudo-words), bodies (limbs and headless bodies), and objects (guitars and cars). Each image was shown only once during the experiment. In each 4 s block, different stimuli of one of the above categories were shown at a rate of two images per second. Blocks were counterbalanced across categories and also with baseline blocks consisting of a blank, gray background. *Oddball task:* During the scan, participants fixated on a central dot and pressed a button when a phase-scrambled oddball image appeared randomly in a block (~33% of the blocks). Data from each human participant were corrected for within-run and between-run motion. Only runs with a motion of less than two voxels were included in the study.

Analysis of Functional Data

Localizer data were analyzed using code written in MATLAB with the mrVista toolbox (https://github.com/vistalab/vistasoft). Data were not spatially smoothed and were analyzed in each participant's native brain space. The time courses of each voxel were converted from arbitrary scanner units into units of % signal change. For each participant, we ran a general linear model (GLM) to model each voxel's time course. The experimental design matrix was convolved with the SPM hemodynamic response function (HRF) (http://www.fil.ion.ucl.ac.uk/spm) to generate predictors. Using a GLM to fit the predictors to the data, we estimated the response amplitudes for each condition (betas) and residual variance of each voxel's time course. We used beta values and residual variance from the GLM to generate contrast maps comparing responses in different conditions.

Definition of Functional Regions of Interest (fROIs)

As in our previous work (Gomez et al. 2017; Weiner et al. 2018; Natu et al. 2019), spatially contiguous clusters of place-selective voxels that responded more strongly to places (houses and indoor scenes) than to all other stimuli in the medial VTC were defined as CoS-places (also referred to as the parahippocampal place area (PPA; Epstein and Kanwisher 1998).

Data Acquisition in Macaques (Anatomical Scans)

For macaque anatomical scans, whole-brain structural volumes were acquired in a 3 T Skyra scanner while the animals were anesthetized with a combination of ketamine (4 mg/kg) and dexdomitor (0.02 mg/kg) and using a 15-channel transmit/receive knee coil. Monkeys were scanned using a magnetization-prepared rapid gradient echo (MPRAGE) sequence; $0.5 \times 0.5 \times 0.5$ resolution; FOV = 128 mm; 256×256 matrix; TR = 2700 ms; TE = 3.35 ms; TI = 859 ms; flip angle = 9°). Three whole-brain T1-weighted anatomical images were collected in each animal.

Reconstruction of Cortical Surfaces

Each animal's T_1 images were also co-registered and averaged. Each monkey's average anatomical volume underwent semi-automated cortical surface reconstruction using FreeSurfer. To ensure high accuracy, skull stripping and white matter masks were first manually segmented by an expert and then passed into FreeSurfer's auto-segmentation pipeline. If poor segmentations were detected, the white matter mask and control points were edited, and surface reconstruction was rerun until corrected. To fix segmentation errors, average anatomical volumes were manually edited to improve the gray/white matter contrasts and to remove surrounding non-brain structures (e.g., sinuses, arachnoid, and dura matter). For all monkeys, auto-segmentation of our main region of interest (occipitotemporal sulcus) was determined to not require manual editing of the anatomical volumes.

Functional Scans

During functional scans, monkeys were alert, and their heads were immobilized using a foam-padded helmet with a chinstrap. Monkeys were rewarded with juice for maintaining a central fixation within a 2° window. Gaze direction was monitored using an infrared eye tracker (ISCAN). Monkeys were scanned in a 3 T TimTrio scanner with an AC88 gradient insert using four-channel surface coils (custom made by Azma Mareyam at the Martinos Imaging Center). We used a T2*-sensitive gradient echo planar pulse sequence with a repetition time (TR) of 2 s, echo time (TE) of 13 ms, flip angle of 72°, slice acceleration (ipat) = 2, 1 mm isotropic voxels, matrix size 96×96 mm, and 67 contiguous sagittal slices. To enhance contrast (Vanduffel et al. 2001; Leite et al. 2002), we injected 12 mg/kg monocrystalline iron oxide nanoparticles (Feraheme, AMAG Pharmaceuticals) in the saphenous vein just before scanning. Monkeys participated in 18–49 runs of a functional localizer experiment with 20 s stimulus blocks and 20 s of a neutral gray screen between image blocks. Monkeys viewed gray-scale stimuli, which were blocked by category. Images consisted of four categories: scenes (familiar

laboratory scenes), faces (mosaics of monkey faces on a pink-noise background), bodies (mosaics of headless monkey bodies on a pink-noise background), and inanimate objects (mosaics of objects on a pink-noise background). Each image subtended 20° × 20° of visual angle and was presented for 0.5 s. Each category block was presented once per scan. Blocks were presented in counterbalanced order across runs. All images were equated for spatial frequency and luminance using the SHINE toolbox (Willenbockel et al. 2010).

Analysis of Functional Data

We analyzed data from the functional localizer experiment as previously reported (Arcaro and Livingstone 2017) using Analysis of Functional NeuroImages (AFNI; Cox 1996), SUMA (Saad and Reynolds 2012), JIP Analysis Toolkit (written by Joseph Mandeville), and MATLAB. For each monkey, all images from each scan session were corrected for within-run and between-run motion. Data were detrended and spatially filtered using a Gaussian filter of 2 mm full-width at half-maximum to increase the signal-to-noise ratio while preserving spatial specificity. Functional volumes were registered to high-resolution (0.5 mm) T1-weighted anatomical images using a two-step linear and then nonlinear approach (JIP Analysis Toolkit) in a two-step process. First, a 12-parameter affine registration was performed between the mean EPI image for a given session and a high-resolution anatomical image. Next, a nonlinear, diffeomorphic registration was performed. Functional data were registered to both participant-specific anatomical images collected in a separate scan session and a group average template (NIH Macaque Template (NMT) (Seidlitz et al. 2018); https://afni.nimh.nih.gov/NMT). For each monkey's data, a multiple regression analysis (AFNI's 3dDeconvolve; Cox 1996) in the framework of a general linear model (Friston et al. 1995) was performed. Each stimulus condition was modeled with a MION-based hemodynamic response function (Leite et al. 2002). Additional regressors that accounted for variance due to baseline shifts between time series, linear drifts, and head motion parameter estimates were also included in the regression model. Due to the time course normalization, beta coefficients were scaled to reflect percent signal change. Because MION inverts the signal, the sign of the beta coefficients was inverted to follow normal fMRI conventions of increased activity represented by positive values.

Definition of fROIs (LPP, Lateral Place Patch)

Functionally selective voxels were defined as clusters of voxels (>10 adjacent voxels) that responded more to images of scenes than to images of other categories ($P < 0.0001$, FDR-corrected). A contrast to faces was not used because three monkeys were raised without visually experiencing faces for the first year of life. For the remaining six monkeys that experienced faces during early development, a contrast between responses to scenes and faces yielded qualitatively similar results.

Generation of Sulcal Depth Maps

For each participant (human and macaque), FreeSurfer's automated algorithm was used to obtain sulcal depth maps. At each vertex along the surfaces, sulcal depth (in mm) is measured as the distance between the inflated and white surfaces obtained from FreeSurfer (Fischl, Sereno, Dale, et al. 1999a, Fischl, Sereno, Tootell, et al. 1999b) using the "mris_inflate" function. It is evaluated using a signed dot product of the displacement/movement vector with the outward pointing surface normal of the white matter surface during inflation. Thus, for a sulcus, the movement vector points outward (toward the pial surface), and therefore, the product is positive. Comparatively, for a gyral crown, the movement vector points inward and, therefore, is negative. Each participant's sulcal depth maps (.sulc files) from the FreeSurfer's auto-segmentation algorithm were used to obtain depth measures from anatomical parcellations of the collateral sulcus (CoS) in humans and the occipitotemporal sulcus (OTS) in macaques. We measured the depth of the sulcal pit in the medial VTC that overlapped with a place-selective region in macaques, as well as human children and adults. We then evaluated the developmental and species differences in the depth of the place-selective sulcal pit using 1) a two-way ANOVA with species (humans/macaques) and hemisphere (left/right) as factors and 2) a two-way ANOVA with age of subject (in humans: child/adults) and hemisphere (left/right) as factors.

Generation of Surface Area and Curvature Values

FreeSurfer's segmentation algorithm was also used to generate the overall curvature of the CoS and its surface area at both pial and white matter surfaces. The overall curvature quantifies the average curvature magnitude of the entire sulcal or gyral fold.

Probabilistic Group Maps of Place Selectivity and Sulcal Depth

To visualize the probabilistic location of place-selective functional ROIs (fROIs) on the cortical sheet, we generated probabilistic group maps of CoS-places in children ($N = 26$) and adults ($N = 28$) separately using cortex-based alignment (CBA) to the FreeSurfer average cortical surface (Fischl, Sereno, Dale, et al. 1999a, Fischl, Sereno, Tootell, et al. 1999b) (Fig. 1). We then calculated the percentage of subjects in which CoS-places overlapped at each vertex on the surface (Fig. 1*b*,*c*). To visualize how the sulcal depth of the CoS varied on the cortical sheet within participants of an age group, we generated probabilistic group maps of the sulcal depth of the CoS also using CBA separately for children and adults. Here, we 1) transformed each participant's sulcal depth maps into FreeSurfer's average cortical space, 2) normalized the transformed maps based on the deepest points of the CoS, 3) added the normalized values at each point of the surface, and 4) divided them by the total number of participants in each group. Then, we obtained the percentage of subjects included in each vertex on the surface. In macaques ($N = 9$), the probability maps of place-selective fROIs (Fig. 1*a*) and sulcal depth maps of the OTS were generated using a macaque average cortical surface template (NMT template from 31 independent macaque brains; Seidlitz et al. 2018) and a procedure identical to that used for humans.

For visualization, we also overlapped each place-selective region with each individual subject's normalized depth maps (normalized to the deepest point in the sulcal fold) thresholded at 80%. We implemented this approach as it is common practice to localize a basin, or cluster, of the deepest points together as the sulcal pit (as opposed to a single point) with MR/cortical surface reconstructions as in previous studies (Im and Grant

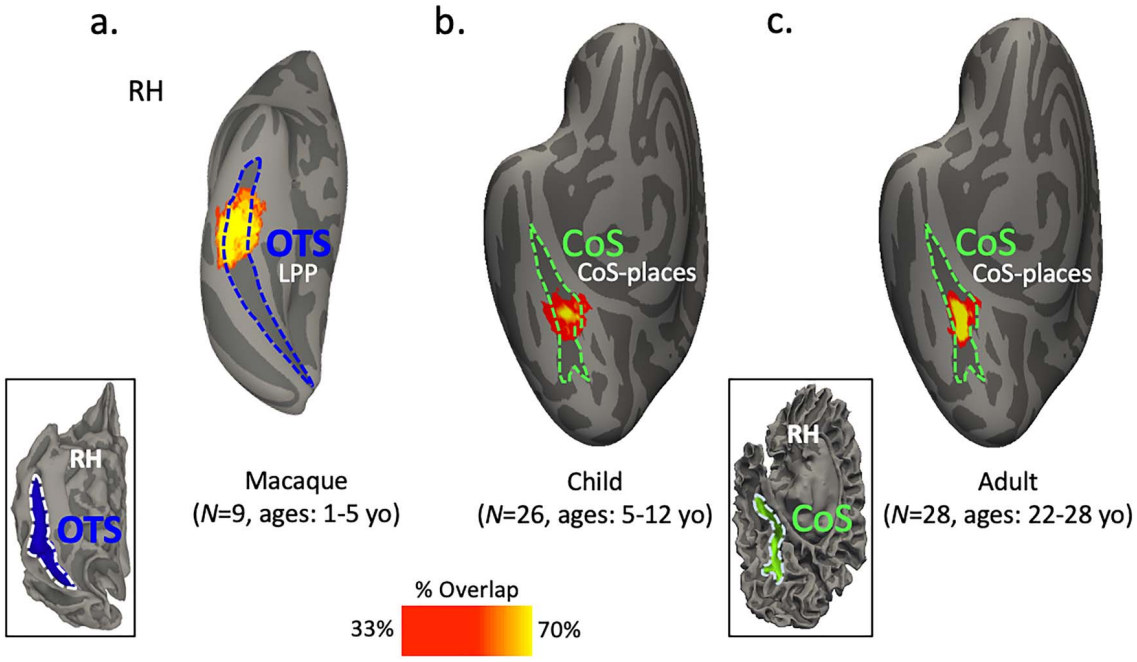

Figure 1. Probabilistic maps of a functionally defined place-selective region in macaques and humans are located within a sulcus in the medial ventral temporal cortex (VTC) across species. (*a*) Inflated cortical surface reconstruction of the right hemisphere of a macaque (NMT; Seidlitz et al. 2018). The map indicates the most probable location of the lateral place patch (LPP) in nine macaques. The most probable location (yellow) is within the occipitotemporal sulcus (OTS; blue). (*b*) Inflated cortical surface reconstruction of the right hemisphere of a human anatomical template (the FreeSurfer average brain from 39 independent adult brains (Fischl, Sereno, Dale, et al. 1999a, Fischl, Sereno, Tootell, et al. 1999b) showing the probabilistic location of CoS-places (also known as the PPA; Epstein and Kanwisher 1998) in 26 children. The most probable location (yellow) of CoS-places is within the collateral sulcus (CoS; green). (*c*) Same as (*b*), but for 28 human adults. Like children, the most probable location (yellow) of CoS-places is within the CoS (green). Warmer colors in the probabilistic maps represent greater overlap of place selectivity across participants within a group. Abbreviations: RH, right hemisphere; CoS, collateral sulcus; OTS, occipital temporal sulcus. Brain sizes not to scale.

2019, Meng et al. 2014, Auzias et al. 2015; Leroy et al. 2015; Bodin et al. 2018).

Generation of Profiles of Sulcal Depth and Selectivity in Humans and Macaques

For each human and macaque, we generated depth and selectivity profiles along the posterior–anterior (e.g., long) axis of the sulcus of interest (CoS in humans and OTS in macaques). This was accomplished by dividing the sulcus into *N* points based on the number of the z-coordinates (representing the posterior–anterior axis) along the length of the sulcus. For each z-coordinate, we averaged the depth/selectivity measures along the x- (lateral–medial) and y-(superior–inferior) planes to obtain depth and selectivity profiles along the sulcus. Specifically, we averaged all the cortical points in a plane orthogonal to the z-axis for each z-point. The number of z-axis points varied between species and hemispheres due to differences in length of the CoS and OTS between species and hemispheres, as well as differences in the resolution of the anatomical scans (0.5 mm^3 isotropic in macaques and 1 mm^3 isotropic in humans). Hence, there were 53 (LH) and 56 (RH) points in the human CoS, as well as 121 (LH) and 125 (RH) points in the macaque OTS, respectively. We then evaluated the structural–functional relationship by correlating depth and selectivity profiles in each individual participant using Pearson's correlation coefficient (R). Finally, we compared the degree of correspondence across species and human development by z-transforming the correlation coefficient and conducting two ANOVAs: one with species (humans/macaques) and hemisphere (left/right) as factors and another with age of subject (in humans: child/adults) and hemisphere (left/right) as factors.

Results

A Functionally Defined Place-Selective Region Is Located within a Sulcus in the Medial VTC across Species

To examine the consistency of the anatomical location of the functionally defined place-selective region across individuals and species, we generated group probabilistic maps of place selectivity by aligning cortical surfaces from each brain to their respective surface templates (FreeSurfer average brain from 39 independent adult brains (Fischl, Sereno, Dale, et al. 1999a, Fischl, Sereno, Tootell, et al. 1999b) for humans; the NMT template from 31 independent macaque brains (Seidlitz et al. 2018) for macaques). Results revealed that in macaques, children, and adults, the place-selective ventral visual region is consistently located within a sulcus in the medial VTC. Due to cortical expansion across evolution (Hill et al. 2010), the sulcus in which the place-selective region is located differs between species. In macaques, the lateral place patch (LPP) is located within the occipitotemporal sulcus (OTS; Fig. 1*a*). In humans, the place-selective region (CoS-places) is located within the collateral sulcus (CoS; Fig. 1*b*,*c*).

The Deepest Sulcal Points (Sulcal Pit) in the Medial Ventral Temporal Cortex Are in Similar Positions across Individuals

Given the consistency in the location of the place-selective region within a sulcal fold in the medial VTC, we next sought to test if the deepest points of the sulcal fold (known as the sulcal pit) are also anatomically consistent. We aligned each individual participant's sulcal depth map (Fig. 2*a*, for sample macaque and human sulcal depth maps) to the average surface template of their respective species and generated a probabilistic map of sulcal depth across participants. This approach revealed that within each group, the locations of the deep sulcal points were well aligned across participants (Fig. 2*b*, warmer colors indicate greater overlap of deep sulcal points across each group). Projecting the location of the sulcal pit (e.g., coordinates of the vertex with the deepest depth) from individual subjects to the average cortical surface revealed that the locations of the deep sulcal pits are largely clustered in close proximity across individual subjects (Fig. 2*b*, see inset and Supplementary Fig. 1 for both hemispheres). Individual sulcal pits were largely constrained (macaque: $N = 8/9$ (RH), $N = 9/9$ (LH), children: $N = 22/26$ (RH), $N = 22/26$ (LH); adults: $N = 25/28$ (RH), $N = 27/28$ (LH)) within the probabilistic place-selective region in both species (dotted white lines in Fig. 2*b*, inset), which we further quantify in subsequent sections.

There is a Consistent Anatomical–Functional Relationship between Sulcal Depth and the Location of the Place-Selective Region in Humans and Macaques

In both species, the sulcus within which the place-selective region is located extends nearly from the occipital to the temporal pole. Given the functional consistency of the place-selective regions across species (Fig. 1), as well as the anatomical consistency of the deepest sulcal points across individuals within each species (Fig. 2*b*), we examined the overlap between each place-selective region and sulcal depth map across groups, as well as in each individual. In all groups (macaques, children, and adults), the place-selective region overlaps the deepest points of the sulcus in the medial VTC (Fig. 2*b*, white dotted line). Specifically, 94.4% of the OTS pits in macaques, 84.6% of the CoS pits in human children, and 92.9% of the CoS pits in human adults are located within the probabilistic place-selective region across both hemispheres (Fig. 2*b*, see inset and Supplementary Fig. 1). Importantly, this structural–functional relationship was also present at the individual subject level (Fig. 2*c* for sample individual subjects; Supplementary Figs 2–4 (for the right hemisphere) and Supplementary Figs 5–7 (for the left hemisphere) for all subjects). Across both left and right hemispheres, in 88.8% of monkeys and in 76.9% of humans (children and adults), the sulcal pit is located within their individual place-selective region. Interestingly, however, the structural–functional overlap was more consistently observed in human adults (85.7%) than in children (68.0%). Thus, the sulcal pit is an anatomical marker that is a good predictor for the location of place selectivity along the anterior–posterior axis of the OTS in macaques and CoS in humans even as the degree of coupling increases from childhood to adulthood.

Sulcal–Functional Relationship Strengthens from Childhood to Adulthood with Additional Evidence that it is Preserved between Macaques and Humans

To further explore the relationship between sulcal depth and place selectivity across development and species, we generated depth and place selectivity profiles along a posterior–anterior axis of each respective sulcus (CoS for humans and OTS for macaques; Materials and Methods). Qualitative examination of the average profiles revealed three main findings. First, we observed that in both macaques and humans, sulcal depth (Fig. 3*a*,*c*) and place selectivity (Fig. 3*b*,*d*) have relatively smooth group average profiles, with a single peak (represented by *). Second, average selectivity and average depth profiles are well aligned in macaques, children, and adults. Specifically, mean place selectivity increases as the sulcus deepens (Fig. 3 and Supplementary Fig. 8 for the right and left hemispheres, respectively). Further, in both adults and macaques, the peak of selectivity (represented by * in Fig. 3*b*,*d* and Supplementary Fig. 8*b*,*d*) is within the deepest region in the sulcus (represented by the gray bar in Fig. 3*a*–*d* and Supplementary Fig. 8*a*,*c*). Third, there are clear developmental differences across human children and adults: In children, but not adults, the mean peak place selectivity was outside but immediately adjacent to the sulcal pit (Fig. 3*d*, peak of the blue line vs. gray bar).

To directly quantify this structural–functional correspondence, we calculated the correlation between each individual's depth and selectivity profiles. This approach revealed that across hemispheres, functional–structural profiles were significantly ($P < 0.05$) positively correlated in 88.9% of the macaques ($N_{left} = 8/9$, $N_{right} = 8/9$; 83.3% when corrected for multiple comparisons). In humans, the functional–structural profiles were significantly and positively correlated in 85.7% of the adults ($N_{left} = 24/28$; $N_{right} = 24/28$; 82.1% when corrected for multiple comparisons) and 67.3% of the children ($N_{left} = 16/26$; $N_{right} = 19/26$; 55.7% children when corrected for multiple comparisons; see Supplementary Figs 9–11 for individual macaque and human functional selectivity and depth profiles, as well as their correlations).

To test if these developmental and species differences are statistically significant, we Fisher z-transformed all correlation coefficients and then compared these correlations using an ANOVA. When collapsing across age groups, the correspondence between sulcal depth and place selectivity was not significantly different between species (macaques ($M_{zscore \pm sem}$): 0.47 ± 0.09; humans: 0.55 ± 0.04, $F_{1,122} = 0.56$, $P > 0.05$. Additionally, within humans, the correspondence between sulcal depth and place selectivity significantly differed between children and adults (children: 0.46 ± 0.06 adults: 0.63 ± 0.05; significant main effect of age: $F_{1,104} = 5.12$, $P < 0.05$). Adults showed stronger coupling between sulcal depth and place selectivity, as well as less variability in the structural–functional coupling compared to children. We find no hemispheric effect across development or species ($Fs < 1.17$, $Ps > 0.05$). In macaques, while they did vary in age, we were unable to test for developmental effects due to the relatively small number of subjects ($N = 9$).

To determine if the structural–functional coupling in and around the sulcal pit is driving the correlation, we used a sliding window approach to calculate the correlation of selectivity and depth into three separate bins: 1) posterior to the sulcal pit, 2)

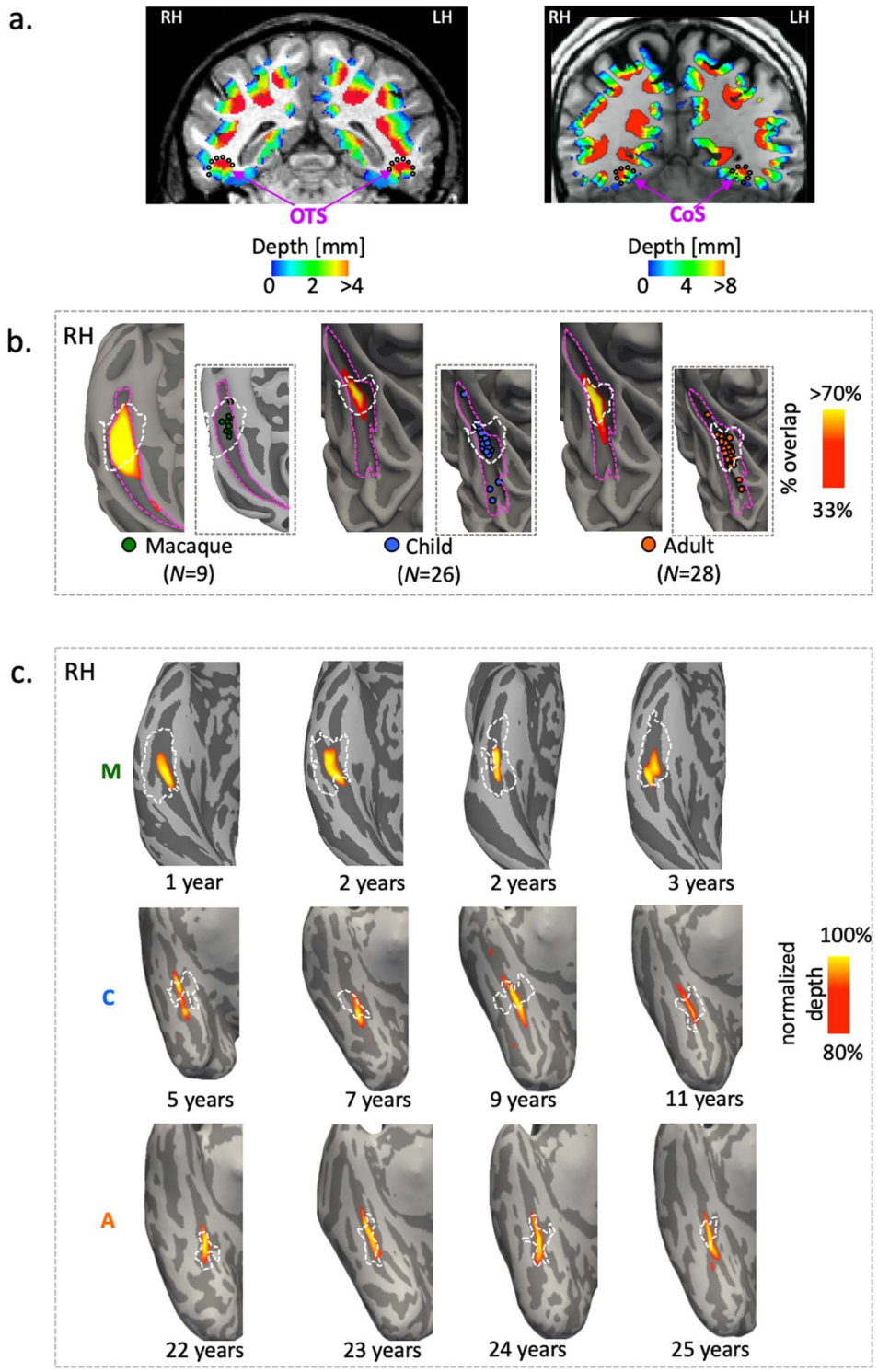

Figure 2. A place-selective region in the medial VTC overlaps the deepest sulcal points in macaques, children, and adults. (*a*) Coronal slices showing depth maps obtained from FreeSurfer's auto-segmentation algorithm in sample macaque and human adult brains (warmer colors represent deeper). For simplicity, the map has been thresholded to only show positive depth values representing sulcal folds, walls, and pits. (*b*) Inflated cortical surfaces of a right hemisphere showing probabilistic maps (percent overlap) of sulcal depth across participants within each group (macaque, children, and adults) at each point of the occipitotemporal sulcus (OTS) in macaques and the collateral sulcus (CoS) in humans (magenta dotted outlines). The locations of the sulcal pit from each individual subject (colored circles) is shown in the inset on the right of each group surface. In each group, deep sulcal points (warmer colors) within the middle of the sulcus overlap the most across individuals. Additionally, probabilistic locations of the place-selective region (dotted white lines obtained from maps in Fig. 1) overlapped with the probabilistic sulcal depth maps (warm colors) in macaques, children, and adults. (*c*) Four sample macaque (top row), child (middle row), and adult (bottom row) ventral temporal surfaces, showing the overlap between the functionally defined place-selective region (white dotted lines) and sulcal depth maps (warm colors). To visualize the deep points of the sulcus, the depth maps in each individual subject are thresholded at 80% depth (100% is the deepest point within the sulcus in each individual). Warmer colors indicate deeper sulcal points. All individual surfaces are shown in Supplementary Figures 2–7. Brain sizes are not to scale.

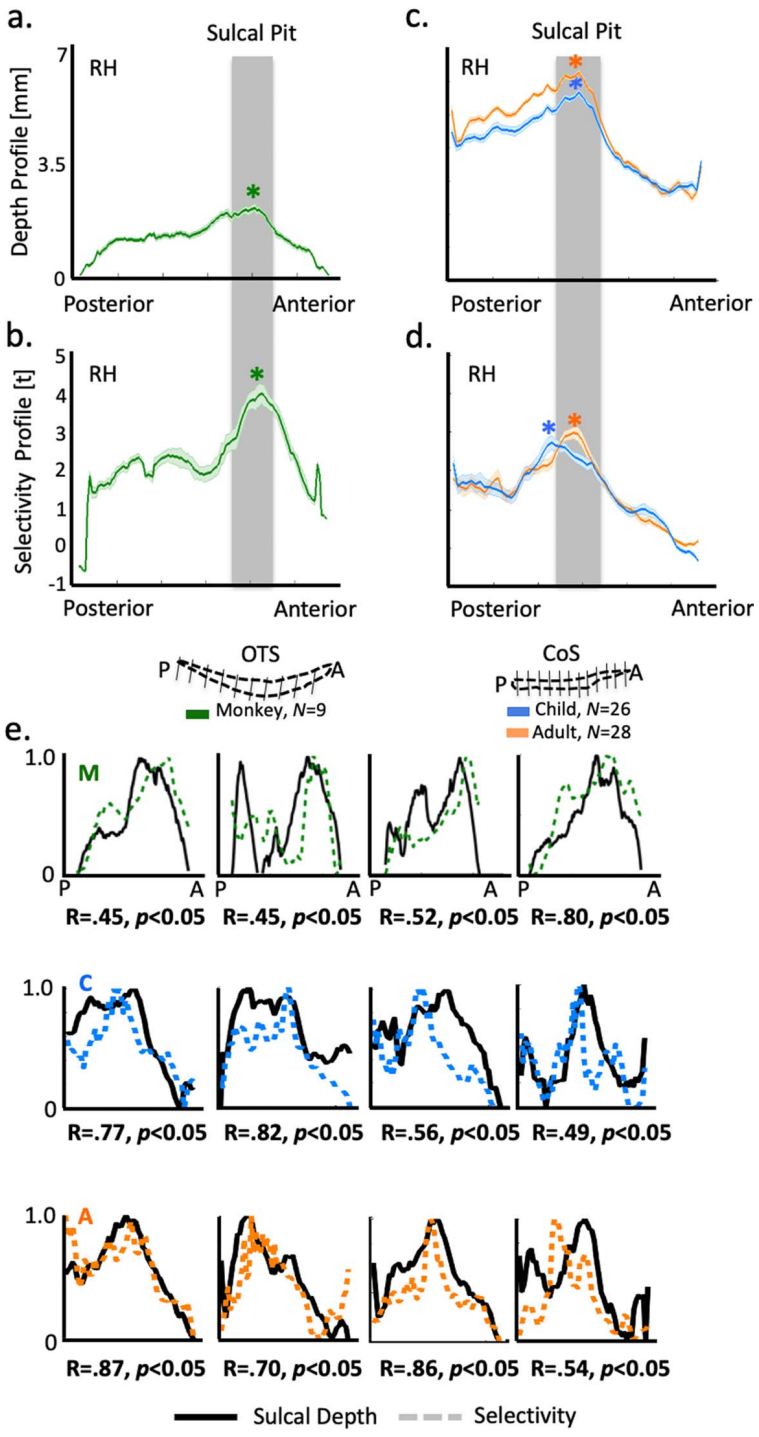

Figure 3. Sulcal depth and place selectivity in the medial VTC are correlated in both humans and macaques. (*a*, *c*) Mean (dark line) and standard deviation (lighter shading) of sulcal depth along the anterior–posterior length of the right OTS in nine macaques (*a*) and the right CoS in humans (*c*). In (*c*), data are averaged across 26 children (blue) and 28 adults (orange). Star (*)represents deepest sulcal point. (*b*, *d*) Mean place selectivity (*t*-value) in macaques (*b*, green) and humans (*d*, blue/orange). Across macaques and humans, the profiles are well-matched along the anterior–posterior axis in which there is a functional peak (represented by * in *b*, *d*) around the deepest sulcal points (represented by gray bar). Left hemisphere data in Supplementary Fig. 8. (*e*) Normalized depth (black lines) and selectivity (colored dotted lines) values as a function of distance along the posterior (P) to anterior (A) axis in four sample macaques (top row), human children (middle row), and human adults (bottom row). Correlation (R) and significance values below each subplot relate the depth and selectivity curves to one another. All individual profiles and their respective correlations are in Supplementary Figures 9–11.

within and surrounding the sulcal pit, and 3) anterior to the sulcal pit (no sulcal point overlapped across the three bins). The correlation between sulcal depth and place selectivity was strongest within and surrounding the sulcal pit and then decreased as the distance from the sulcal pit increased on either side of the pit for both hemispheres and species (Supplementary Fig. 12 for left and right hemispheres; macaque: $R_{mean \pm std}$: $M_{close} = 0.62 \pm 0.3$, $M_{away} = 0.24 \pm 0.5$; children: $C_{close} = 0.54 \pm 0.49$, $C_{away} = 0.01 \pm 0.49$; adults: $A_{close} = 0.58 \pm 0.45$, $A_{away} = 0.15 \pm 0.48$). Importantly, we evaluated if these differential effects at deep sulcal depths versus their surrounding areas were driven by a potentially heightened functional response related to greater signal to noise ratio (SNR)—due to presumably less partial voluming effects—at the sulcal fundus (Koo et al. 2009). Measuring the time series signal-to-noise ratio (tSNR = mean(time-series)/std(time-series)) across species showed that this was not the case. Regions around the deep sulcal depths do not show the highest tSNR in our data (Supplementary Fig. 13). Furthermore, in humans, although we find stronger sulcal–functional coupling in adults compared to children (which would predict higher tSNR in adults compared to children), we find the opposite: There is larger tSNR in children than adults along the entire length of the CoS (Supplementary Fig. 13*d*).

Finally, to examine a stringent sulcal–functional mapping not commonly implemented in previous studies (Im et al. 2010; Meng et al. 2014; Leroy et al. 2015; Auzias et al. 2015; Bodin et al. 2018), we also tested if the single deepest point predicted the single point with the highest place selectivity. To do so, we measured the distance between the single deepest sulcal point and the single voxel with the highest place selectivity using the FreeSurfer function "mris_pmake," which calculates the distance between two vertices on a cortical surface map. The approximate peak-to-peak distance is ~0.5 cm in macaques ($M = 4.97$ mm, Std: 2.61 mm), ~1.5 cm in human children (M: 15.39 mm, Std: 10.13 mm), and ~1 cm in human adults (M: 10.5 mm, Std: 7.04 mm). An ANOVA with species (humans/-monkeys) and hemisphere (left/right) as factors revealed a main effect of species ($F_{1,122} = 16.2$, $P < 0.05$). Additionally, an ANOVA with age group (child/adult) and hemisphere as factors also showed a main effect of age ($F_{1,104} = 5.5$, $P < 0.05$), in which there was a tighter coupling between the deepest point and most selective voxel in adults compared to children. Altogether, these results reveal that the anatomical landmark of the sulcal pit is functionally relevant within the medial VTC across species. Furthermore, within humans, the structural–functional coupling between sulcal depth and place selectivity becomes stronger and more stable from childhood to adulthood.

What Underlying Mechanisms May Contribute to the Stronger Coupling between Sulcal Depth and Place Selectivity in the Medial VTC from Childhood to Adulthood in Humans?

Prior results suggest that age-related cortical thinning in CoS-places in humans is linked to the morphological changes in its curvature (Natu et al. 2019). Thus, we explored the possibility that developmental changes in sulcal fold morphology may also contribute to the structural–functional correspondence in the CoS. For example, the CoS may deepen with age, and this deepening may push the functional region toward the fundus of the sulcus. Indeed, comparing CoS depth across age revealed that the CoS is deeper in adults than in children (main effect of age in a two-way ANOVA with factors age of subject (child/adult) and hemisphere (left/right): $F_{1,104} = 15.59$, $P < 0.001$, Fig. 4*a*,*b*). On average, the depth of the CoS sulcal pit in human adults is 10.5 ± 0.18 mm, which is ~8.5% deeper than in human children (9.65 ± 0.23 mm, Fig. 4*b*). Intriguingly, this is not the case for all sulci. For example, in both children and adults, the deepest point is found in the insula, and there is no age-related deepening in this sulcal pit from age 5 to adulthood (no main effect of age of subject: $F_{1,104} = 3.7$, $P > 0.05$).

To further explore changes to the sulcal morphology that occur with this deepening, we examined if mean curvature and surface area in the upper compared to the lower cortical surfaces of the CoS also develop from childhood to adulthood. To do so, we measured the mean curvature of the CoS at the pial (upper) and white (lower) matter surfaces as prior studies suggest that differential changes in the upper versus lower cortical surfaces may result in gyrification and sulcal deepening of the cortex (Richman et al. 1975; Ronan et al. 2004). This approach revealed that the curvature at the pial surface is greater than that at the white matter surface in the CoS across age groups ($F_{1,208} = 764.9$, $P < 0.001$, Fig. 4*c*) and also that curvature develops with age. Specifically, while there is no development of the curvature at the white matter surface, the overall mean curvature at the pial surface decreased from childhood to adulthood (significant interaction between age and surface type: $F_{1,208} = 56.03$, $P < 0.001$, Fig. 4*c*). Additionally, there was also significant age-related surface area expansion of both pial and white matter surfaces across hemispheres (main effect of age; $F_{1,208} = 18.77$, $P < 0.001$). Together, these results demonstrate that differential developmental changes occur at the pial and white matter surfaces of the collateral sulcal fold in humans from childhood to adulthood.

Discussion

Using comparative fMRI in macaques and humans (both children and adults), we examined the relationship between deep sulcal points and functionally specialized regions that are critical for processing visual scenes and places in the medial ventral temporal cortex (VTC). Our results revealed three main findings. First, place-selective regions in the medial VTC overlap the deepest points (e.g., sulcal pits) along the OTS in macaques and the CoS in humans (Figs 1 and 2). Second, more broadly, there is a strong relationship between sulcal depth and place selectivity across age groups and species in which deeper points have higher place selectivity in the human CoS as well as in the macaque OTS. Nevertheless, the strongest correlation between depth and selectivity occurred at the location of the sulcal pit and surrounding cortex in the sulcal fold (Fig. 3). Third, the coupling between sulcal pits and place-selective regions in the medial VTC strengthens from childhood to adulthood (Fig. 3). Mechanistically, we propose that sulcal deepening and differential changes in the cortical curvature of the pial and white matter surfaces contribute to the strengthening of this sulcal–functional coupling from childhood to adulthood (Fig. 4). In the sections below, we discuss our findings in the context of 1) sulcal features as functional landmarks in high-level visual cortex in gyrencephalic brains and 2) the role of sulcal deepening and cortical surface expansion as underlying mechanisms contributing to the observed sulcal–functional coupling in the medial VTC across development and species.

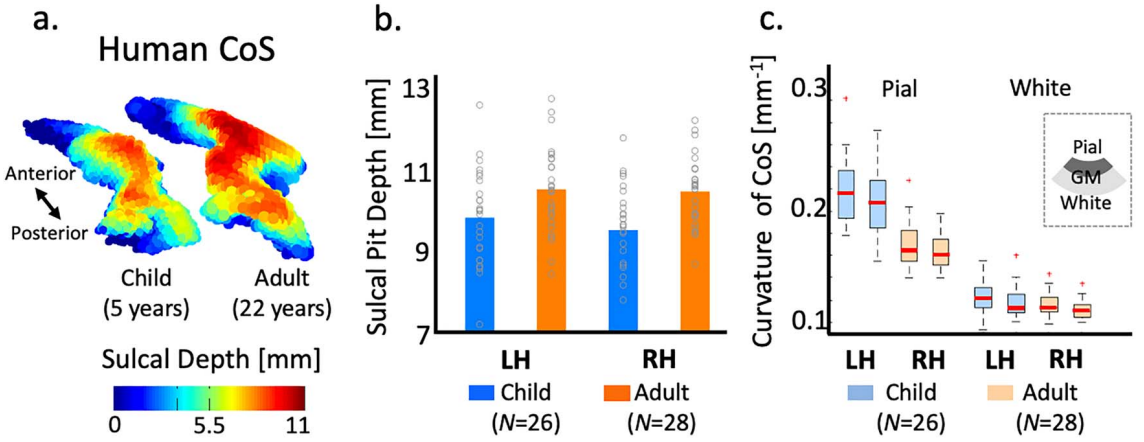

Figure 4. Morphological differences in the CoS between children and adults. (*a*) Three-dimensional sulcal depth maps of the CoS in an example child (5 years old) and adult (22 years old) showing differences in depth (represented by increasing height of the 3D maps). (*b*) Mean depth of place-selective sulcal pits in children (blue) and adults (orange). Gray circles: individual subjects. (*c*) Box plots showing median (thick red line), 25th and 75th percentile (box), and range (whiskers) of curvature of the CoS at the pial and white matter surfaces in children (blue) and adults (orange). GM, gray matter. LH, left hemisphere. RH, right hemisphere.

Sulcal Features as Functional Landmarks in the High-Level Visual Cortex in Gyrencephalic Brains: Methodological, Behavioral, and Theoretical Implications

Our results showing that there is a tight correspondence between the location of sulcal pits in the medial VTC and place selectivity in both macaques and humans, as well as in children and adults, are surprising because these place-selective regions are located in high-level visual cortex. Previous theories of cortical folding (Richman et al. 1975; Welker 1990; Armstrong et al. 1995; Van Essen 1997; Toro and Burnod 2005; Zilles et al. 2013) would predict a tight sulcal–functional relationship between a primary sulcus in the visual cortex (i.e., the calcarine sulcus) and a primary visual area (V1). It is unclear that such sulcal–functional relationships would exist in high-level visual regions where sulcal folds are more complex and vary across individuals and primate species. Thus, these theories would not predict that 1) deep sulcal points located in what is considered one of the last stages of the visual processing hierarchy would predict the strongest selectivity of a high-level region selective for visual scenes, 2) this sulcal–functional coupling would occur in both macaques and humans, or c) this sulcal–functional coupling would strengthen from childhood to adulthood—each of which we show in the present study. This latter point is particularly striking as one might expect structure–function relationships to be established early in development (potentially by genetic markers) and, thus, largely fixed.

The combination of these results further illustrates the utility of sulcal features as functional landmarks in high-level visual cortex in gyrencephalic brains. For example, previous research in humans showed that 1) the anterior tip of the mid-fusiform sulcus accurately identifies a region selective for faces (Weiner and Grill-Spector 2010: Weiner et al. 2014), as well as 2) a sulcal intersection between two sulci in the medial VTC accurately identifies the location of a region selective for visual places and scenes (Weiner et al. 2018). One might question the role of relatively small sample sizes when identifying these structural–functional relationships. In our previous work, we showed that a predicted location of CoS-places predicted the cortical location of voxels exhibiting the highest functional place selectivity in over 500 participants from the Human Connectome Project (HCP) (Weiner et al. 2018). Furthermore, a recent study by Abbasi et al. (2020) examined fMRI data of 424 adults (212 twin pairs) also from the HCP database to determine the relationship between genetics and the organization of category-selective visual cortex. They found that genetic voxels were preferentially concentrated in regions with higher cortical curvature: sulcal fundi for place-selective regions (consistent with the present results reported here) and gyral crowns for face-selective regions in the ventral temporal cortex. Given these consistent structural–functional links observed in the relatively diverse and large-scale HCP dataset, we anticipate that the strong sulcal–functional relationship we report here will generalize to a randomly selected, large-scale, and diverse group of participants. Furthermore, our work extends the structural–functional relationship identified previously (Weiner et al. 2018) to a specific morphological feature of sulcal depth, which is consistent with recent work showing that a sulcal pit within the human STS predicts the location of a functional region processing human voices (Bodin et al. 2018). Together, these findings suggest the possibility that a subset of functional regions in gyrencephalic brains are likely identifiable simply from anatomical features such as sulcal depth maps instead of functional localizer experiments, which can be examined in future work.

Additional future work will likely build on this correspondence between sulcal features and functional selectivity to also incorporate aspects of behavior and cognition. For instance, sulcal interruptions in human lateral VTC have been shown to predict the location of regions selective for words as well as correlate with reading ability (Cachia et al. 2018). Furthermore, the depth of sulcal pits is correlated with different aspects of cognition such as verbal IQ (Im et al. 2011), and differences in the cortical depths and morphology of sulci are also well-known markers for developmental neurocognitive disorders such as autism (Auzias et al. 2014; Brun et al. 2016). Finally, significant hemispheric asymmetries in the frequency and distribution of sulcal pits in the superior temporal sulcus (STS) are considered to be human-specific cortical landmarks of language and socio-communication abilities (Im et al. 2010; Auzias et al. 2015; Leroy et al. 2015).

Given this growing body of work showing a relationship between sulcal depth and functional cortical representations, as

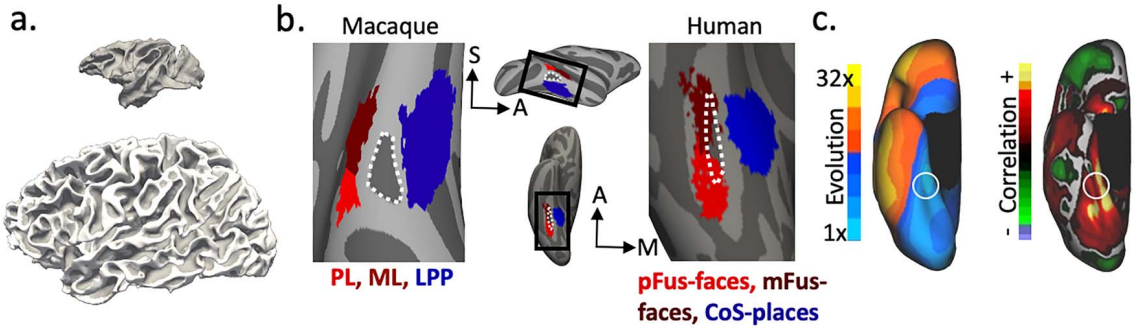

Figure 5. The topology of place- and face-selective regions relative to shallow and deep sulci is relatively preserved in the VTC despite significant differences in brain size and macroanatomy between macaques and humans. (*a*) Sagittal views of a sample macaque and a human brain (to scale) showing that human brains are ~15 times bigger than macaque brains. (*b*) Middle, top: lateral view of the macaque cortical surface (NMT; Seidlitz et al. 2018). Black rectangle: zoomed portion illustrated in the left image showing the macaque face-selective patches ML (maroon) and PL (red) relative to the lateral place-selective patch (LPP; blue). Each patch is the probabilistic location across nine macaques. The zoomed image has been rotated (superior: left of the image; anterior: top of the image). A shallow sulcus (posterior middle temporal sulcus, pmts; dotted white outline) divides ML and PL from LPP. Middle, bottom: ventral view of the human cortical surface (FreeSurfer average template from 39 adults; Fischl, Sereno, Dale, et al. 1999a, Fischl, Sereno, Tootell, et al. 1999b). Black rectangle: zoomed portion illustrated in the right image showing the human face-selective regions (mFus-faces (maroon) and pFus-faces (red)) relative to the place-selective region, CoS-places (blue). Each region is the probabilistic definition across 12 adults from Weiner et al. (2018). A shallow sulcus (mid-fusiform sulcus, MFS; dotted white outline) divides mFus-faces and pFus-faces from CoS-places. (*c*) Left: image of the human brain (from the PALS-B12 atlas) adapted from Hill et al. (2010), with permission. Map shows regional evolutionary cortical expansion between an adult macaque and the average human adult on the right ventral surface. White circle has been added to the original images to indicate the approximate location of CoS-places examined in humans in the present study. Regions in the medial VTC show minimal cortical expansion compared to the remainder of cortex, while the anterior–lateral VTC (warm colors) exhibits much more expansion compared to the medial VTC. Right: the same cortical reconstruction of the right hemisphere with a correlation map between evolutionary and postnatal cortical expansion (adapted from Hill et al. (2010)), with permission. Regions in the medial VTC show a positive correlation across evolutionary and postnatal expansion patterns, while regions in the anterior–lateral VTC show little or a negative correlation. A, anterior; S, superior; M, medial.

well as sulcal depth and human cognition, we believe that our results are theoretically meaningful rather than epiphenomenal. Nevertheless, the commonalities between the functional arealization of the visual cortex more generally across species despite vast differences in brain size, cortical folding, and gyrification (Van Essen 1997; Rosa and Tweedale 2005; Hill et al. 2010; Zilles et al. 2013; Arcaro and Kastner 2015) cannot be ignored as they implicate that sulci may not be necessary for the development of category-selective regions. Thus, while it is beyond the scope of the present study, future theoretical and modeling work of cortical folding relative to functional areas across species should also consider the functional role of sulcal pits in the emergence, development, and evolution of functionally specialized areas specifically in gyrencephalic brains.

Sulcal Deepening and Cortical Surface Expansion: Mechanistic Explanations across Development and Species

Mechanistically, we propose that sulcal deepening and cortical surface expansion are parsimonious principles contributing to the sulcal–functional coupling observed in the present study across development and species. Developmentally, we propose that areal expansion and differential developments of the cortical curvature that occur as the CoS deepens with age likely push the functionally active neurons closer to the sulcal fundus, thereby reducing the interneural distances and stabilizing the relationship between sulcal depth and place selectivity in adulthood. Recent findings showing that place-selective cortex thins from childhood to adulthood complement this mechanistic explanation (Natu et al. 2019). Specifically, the thinning of place-selective cortex is likely linked to the morphological developments identified here in which the sulcal fold stretches and deepens leading to the shift in location of CoS-places from childhood to adulthood.

Evolutionarily, we found that the coupling between place selectivity and sulcal depth in the medial VTC was just as strong in monkeys as in humans (Fig. 3). This is quite surprising given that the size of the human brain is ~15 times that of the macaque brain (Fig. 5*a*) and that other category-selective regions, such as those selective for faces, are located in different anatomical locations across species. For example, two face-selective regions are located on the fusiform gyrus (FG) in human VTC, and macaques do not have an FG. Thus, the face processing system is shifted more dorsolaterally in macaques compared to humans (Tsao et al. 2008; Weiner and Grill-Spector 2015; Arcaro and Livingstone 2017; Fig. 5*b*). Despite this major difference between species, the topological positioning of face- and place-selective regions relative to shallow and deep sulci is consistent: Two face-selective regions (ML and PL in macaque; mFus-faces and pFus-faces in human) are located adjacent to a shallow sulcus (posterior middle temporal sulcus in macaque; mid-fusiform sulcus in human), while a place-selective region (LPP in macaque; CoS-places in human) is located within a deep sulcus (OTS in macaque; CoS in human) across species (Fig. 5*b*).

We propose that evolutionary and postnatal cortical expansion can account for the relationship in the cortical locations of face- and place-selective regions across species. Specifically, prior studies show that both postnatal and evolutionary cortical surface expansions are correlated in the medial VTC (Hill et al. 2010; Fig. 5*c*). Notably, this cortical location has relatively less evolutionary expansion compared to the rest of the cortex, which likely explains the coupling between sulcal depth and place selectivity in the medial VTC across species. On the contrary, the anterior–lateral VTC shows no or a negative correlation between postnatal and evolutionary cortical expansion, as well as greater evolutionary expansion compared to medial VTC (Fig. 5*c*). These evolutionary anatomical differences likely contribute to the fact that category-selective regions are located on different anatomical structures across species. Furthermore,

postnatal anatomical differences between the lateral and medial VTC also align with the protracted development of face-selective regions in the lateral VTC and the early emergence (Deen et al. 2017) and development of place-selective regions in the medial VTC in humans (Golarai et al. 2007, 2010; Gomez et al. 2017; Natu et al. 2019). Future work will determine if this postnatal expansion also contributes to greater individual differences in the location of face-selective regions compared to place-selective regions across age groups and species. Additionally, future work will also determine if the developmental mechanisms underlying the sulcal–functional coupling identified here in the medial VTC are also comparable across species and if they extend to other functional features.

In conclusion, our study provides novel evidence of a homologous macroanatomical–functional relationship between species in which sulcal depth in the medial VTC predicts place selectivity in high-level visual cortex in both humans and macaques. This shared feature implies that this structural–functional relationship has been conserved across evolution. Our study has broad impact as it can be used to provide deeper understanding of finer anatomical–functional relationships in other functional domains across sulcal and gyral folds and, more broadly, to examine these relationships in atypical human brain development as well as other primates.

Supplementary Material

Supplementary material can be found at *Cerebral Cortex* online.

Authors' Contributions

V.S.N. and K.S.W. conceived and designed the analyses relating sulcal depth and place selectivity across species; V.S.N. designed the human fMRI experiment, collected human fMRI data, analyzed human and macaque data, and wrote the manuscript; M.A. and M.L. designed macaque fMRI experiment and collected macaque fMRI data. M.A. analyzed macaque fMRI data and wrote the manuscript; M.A.B. and J.G. contributed to the human fMRI data collection and analysis; K.G.S. and K.S.W. oversaw the components of the human fMRI experiment; K.S.W. wrote the manuscript. All co-authors have read and approved the submitted manuscript.

Notes

Conflict of interest: None declared.

Funding

National Eye Institute (NEI) (grant R01 EY02231801, R01 EY02391501 to K.G.S.); T-32 National Eye Institute Vision Training Fellowship (to V.S.N.), and Start-Up Funds provided by UC Berkeley (to K.S.W.).

References

Abbasi N, Duncan J, Rajimehr R. 2020. Genetic influence is linked to cortical morphology in category-selective areas of visual cortex. *Nat Commun*. 11:709.

Amiez C, Petrides M. 2014. Neuroimaging evidence of the anatomo-functional organization of the human cingulate motor areas. *Cereb Cortex*. 24:563–578.

Amiez C, Sallet J, Hopkins WD, Meguerditchian A, Hadj-Bouziane F, Ben Hamed S, Wilson CRE, Procyk E, Petrides M. 2019. Sulcal organization in the medial frontal cortex provides insights into primate brain evolution. *Nat Commun*. 10:3437.

Amiez C, Wilson CRE, Procyk E. 2018. Variations of cingulate sulcal organization and link with cognitive performance. *Sci Rep*. 8:13988.

Arcaro MJ, Kastner S. 2015. Topographic organization of areas V3 and V4 and its relation to supra-areal organization of the primate visual system. *Vis Neurosci*. 32:E014.

Arcaro MJ, Livingstone MS. 2017. Retinotopic organization of scene areas in macaque inferior temporal cortex. *In J Neurosci*. 37:7373–7389.

Armstrong E, Schleicher A, Omran H, Curtis M, Zilles K. 1995. The ontogeny of human gyrification. *Cereb Cortex*. 5:56–63.

Auzias G, Brun L, Deruelle C, Coulon O. 2015. Deep sulcal landmarks: algorithmic and conceptual improvements in the definition and extraction of sulcal pits. *Neuroimage*. 111:12–25.

Auzias G, Viellard M, Takerkart S, Villeneuve N, Poinso F, Fonseca DD, Girard N, Deruelle C. 2014. Atypical sulcal anatomy in young children with autism spectrum disorder. *Neuroimage Clin*. 4:593–603.

Benson NC, Butt OH, Datta R, Radoeva PD, Brainard DH, Aguirre GK. 2012. The retinotopic organization of striate cortex is well predicted by surface topology. *Curr Biol*. 22:2081–2085.

Benson NC, Manning JR, Brainard DH. 2014. Unsupervised learning of cone spectral classes from natural images. *PLoS Comput Biol*. 10:e1003652.

Bodin C, Takerkart S, Belin P, Coulon O. 2018. Anatomo-functional correspondence in the superior temporal sulcus. *Brain Struct Funct*. 223:221–232.

Brun L, Auzias G, Viellard M, Villeneuve N, Girard N, Poinso F, Da Fonseca D, Deruelle C. 2016. Localized misfolding within Broca's area as a distinctive feature of autistic disorder. *Biol Psychiatry Cogn Neurosci Neuroimaging*. 1:160–168.

Cachia A, Roell M, Mangin JF, Sun ZY, Jobert A, Braga L, Houde O, Dehaene S, Borst G. 2018. How interindividual differences in brain anatomy shape reading accuracy. *Brain Struct Funct*. 223:701–712.

Cox RW. 1996. AFNI: software for analysis and visualization of functional magnetic resonance neuroimages. *Comput Biomed Res*. 29:162–173.

Deen B, Richardson H, Dilks DD, Takahashi A, Keil B, Wald LL, Kanwisher N, Saxe R. 2017. Organization of high-level visual cortex in human infants. *Nat Commun*. 8:13995.

Dumoulin SO, Bittar RG, Kabani NJ, Baker CL, Le Goualher G, Bruce Pike G, Evans AC. 2000. A new anatomical landmark for reliable identification of human area V5/MT: a quantitative analysis of sulcal patterning. *Cereb Cortex*. 10:454–463.

Epstein R, Kanwisher N. 1998. A cortical representation of the local visual environment. *Nature*. 392:598–601.

Feinberg DA, Moeller S, Smith SM, Auerbach E, Ramanna S, Gunther M, Glasser MF, Miller KL, Ugurbil K, Yacoub E. 2010. Multiplexed echo planar imaging for sub-second whole brain FMRI and fast diffusion imaging. *PLoS One*. 5:e15710.

Felleman DJ, Van Essen DC. 1991. Distributed hierarchical processing in the primate cerebral cortex. *Cereb Cortex*. 1:1–47.

Fischl B, Sereno MI, Dale AM. 1999a. Cortical surface-based analysis. II: inflation, flattening, and a surface-based coordinate system. *Neuroimage*. 9:195–207.

Fischl B, Sereno MI, Tootell RB, Dale AM. 1999b. High-resolution intersubject averaging and a coordinate system for the cortical surface. *Hum Brain Mapp*. 8:272–284.

Friston KJ, Frith CD, Turner R, Frackowiak RS. 1995. Characterizing evoked hemodynamics with fMRI. *Neuroimage*. 2:157–165.
Golarai G, Ghahremani DG, Whitfield-Gabrieli S, Reiss A, Eberhardt JL, Gabrieli JD, Grill-Spector K. 2007. Differential development of high-level visual cortex correlates with category-specific recognition memory. *Nat Neurosci*. 10:512–522.
Golarai G, Liberman A, Yoon JM, Grill-Spector K. 2010. Differential development of the ventral visual cortex extends through adolescence. *Front Hum Neurosci*. 3:80.
Gomez J, Barnett MA, Natu V, Mezer A, Palomero-Gallagher N, Weiner KS, Amunts K, Zilles K, Grill-Spector K. 2017. Microstructural proliferation in human cortex is coupled with the development of face processing. *Science*. 355:68–71.
Hasnain MK, Fox PT, Woldorff MG. 2006. Hemispheric asymmetry of sulcus-function correspondence: quantization and developmental implications. *Hum Brain Mapp*. 27: 277–287.
Gomez J, Natu V, Jeska B, Barnett M, Grill-Spector K. 2018. Development differentially sculpts receptive fields across early and high-level human visual cortex. *Nat Commun*. 9:788.
Grill-Spector K, Weiner KS. 2014. The functional architecture of the ventral temporal cortex and its role in categorization. *Nat Rev Neurosci*. 15:536–548.
Hill J, Inder T, Neil J, Dierker D, Harwell J, Van Essen D. 2010. Similar patterns of cortical expansion during human development and evolution. *Proc Natl Acad Sci*. 107:13135–13140.
Hinds OP, Rajendran N, Polimeni JR, Augustinack JC, Wiggins G, Wald LL, et al. 2008. Accurate prediction of V1 location from cortical folds in a surface coordinate system. *Neuroimage*. 39:1585–1599.
Im K, Choi YY, Yang JJ, Lee KH, Kim SI, Grant PE, Lee JM. 2011. The relationship between the presence of sulcal pits and intelligence in human brains. *Neuroimage*. 55:1490–1496.
Im K, Grant PE. 2019. Sulcal pits and patterns in developing human brains. *Neuroimage*. 185:881–890.
Im K, Jo HJ, Mangin JF, Evans AC, Kim SI, Lee JM. 2010. Spatial distribution of deep sulcal landmarks and hemispherical asymmetry on the cortical surface. *Cereb Cortex*. 20: 602–611.
Kolster H, Janssens T, Orban GA, Vanduffel W. 2014. The retinotopic organization of macaque occipitotemporal cortex anterior to V4 and caudoventral to the middle temporal (MT) cluster. *J Neurosci*. 34:10168–10191.
Koo BB, Hua N, Choi CH, Ronen I, Lee JM, Kim DS. 2009. A framework to analyze partial volume effect on gray matter mean diffusivity measurements. *Neuroimage*. 44:136–144.
Kornblith S, Cheng X, Ohayon S, Tsao DY. 2013. A network for scene processing in the macaque temporal lobe. *Neuron*. 79:766–781.
Larsson J, Heeger DJ. 2006. Two retinotopic visual areas in human lateral occipital cortex. *J Neurosci*. 26:13128–13142.
Leite FP, Tsao D, Vanduffel W, Fize D, Sasaki Y, Wald LL, Dale AM, Kwong KK, Orban GA, Rosen BR, et al. 2002. Repeated fMRI using iron oxide contrast agent in awake, behaving macaques at 3 tesla. *Neuroimage*. 16:283–294.
Leroy F, Cai Q, Bogart SL, Dubois J, Coulon O, Monzalvo K, Fischer C, Glasel H, Van der Haegen L, Benezit A, et al. 2015. New human-specific brain landmark: the depth asymmetry of superior temporal sulcus. *Proc Natl Acad Sci*. 112:1208–1213.
Lohmann G, von Cramon DY, Colchester AC. 2008. Deep sulcal landmarks provide an organizing framework for human cortical folding. *Cereb Cortex*. 18:1415–1420.
Lopez-Persem A, Verhagen L, Amiez C, Petrides M, Sallet J. 2019. The human ventromedial prefrontal cortex: Sulcal morphology and its influence on functional organization. *J Neurosci*. 39:3627–3639.
Meng Y, Li G, Lin W, Gilmore JH, Shen D. 2014. Spatial distribution and longitudinal development of deep cortical sulcal landmarks in infants. *Neuroimage*. 100:206–218.
Mezer A, Yeatman JD, Stikov N, Kay KN, Cho NJ, Dougherty RF, Perry ML, Parvizi J, Hua le H, Butts-Pauly K, et al. 2013. Quantifying the local tissue volume and composition in individual brains with magnetic resonance imaging. *Nat Med*. 19:1667–1672.
Nasr S, Liu N, Devaney KJ, Yue X, Rajimehr R, Ungerleider LG, Tootell RB. 2011. Scene-selective cortical regions in human and nonhuman primates. *J Neurosci*. 31:13771–13785.
Natu VS, Barnett MA, Hartley J, Gomez J, Stigliani A, Grill-Spector K. 2016. Development of neural sensitivity to face identity correlates with perceptual discriminability. *J Neurosci*. 36:10893–10907.
Natu VS, Gomez J, Barnett M, Jeska B, Kirilina E, Jaeger C, Zhen Z, Cox S, Weiner KS, Weiskopf N, et al. 2019. Apparent thinning of human visual cortex during childhood is associated with myelination. *Proc Natl Acad Sci*. 116:20750–20759.
Nordt M, Gomez J, Natu V, Jeska B, Barnett M, Grill-Spector K. 2018. Learning to read increases the Informativeness of distributed ventral temporal responses. *Cereb Cortex*. 29: 517–527.
Rajimehr R, Tootell RB. 2009. Does retinotopy influence cortical folding in primate visual cortex? *J Neurosci*. 29:11149–11152.
Rakic P. 1988. Specification of cerebral cortical areas. *Science*. 241:170–176.
Regis J, Mangin JF, Ochiai T, Frouin V, Riviere D, Cachia A, Tamura M, Samson Y. 2005. Sulcal root generic model: a hypothesis to overcome the variability of the human cortex folding patterns. *Neurol Med Chir*. 45:1–17.
Richman DP, Stewart RM, Hutchinson JW, Caviness VS Jr. 1975. Mechanical model of brain convolutional development. *Science*. 189:18–21.
Ronan L, Voets N, Rua C, Alexander-Bloch A, Hough M, Mackay C, Crow TJ, James A, Giedd JN, Fletcher PC. 2004. Differential tangential expansion as a mechanism for cortical gyrification. *Cereb Cortex*. 24:2219–2228.
Rosa MG, Tweedale R. 2005. Brain maps, great and small: lessons from comparative studies of primate visual cortical organization. *Philos Trans R Soc Lond B Biol Sci*. 360:665–691.
Saad ZS, Reynolds RC. 2012. Suma. *Neuroimage*. 62:768–773.
Scherf KS, Behrmann M, Humphreys K, Luna B. 2007. Visual category-selectivity for faces, places and objects emerges along different developmental trajectories. *Dev Sci*. 10: 15–30.
Seidlitz J, Sponheim C, Glen D, Ye FQ, Saleem KS, Leopold DA, Ungerleider L, Messinger A. 2018. A population MRI brain template and analysis tools for the macaque. *Neuroimage*. 170:121–131.
Sereno MI, Tootell RB. 2005. From monkeys to humans: what do we now know about brain homologies? *Curr Opin Neurobiol*. 15:135–144.
Stigliani A, Weiner KS, Grill-Spector K. 2015. Temporal processing capacity in high-level visual cortex is domain specific. *J Neurosci*. 35:12412–12424.
Tootell RB, Hadjikhani NK, Vanduffel W, Liu AK, Mendola JD, Sereno MI, Dale AM. 1998. Functional analysis of

primary visual cortex (V1) in humans. *Proc Natl Acad Sci USA*. 95:811–817.

Toro R, Burnod Y. 2005. A morphogenetic model for the development of cortical convolutions. *Cereb Cortex*. 15:1900–1913.

Tsao DY, Freiwald WA, Knutsen TA, Mandeville JB, Tootell RB. 2003. Faces and objects in macaque cerebral cortex. *Nat Neurosci*. 6:989–995.

Tsao DY, Moeller S, Freiwald W. 2008. Comparing face patch systems in macaques and humans. *PNAS*. 105:19514–19519.

Van Essen DC, Donahue CJ, Coalson TS, Kennedy H, Hayashi T, Bakircioglu M, Glasser MF. 2019. Cerebral cortical folding, parcellation, and connectivity in humans, nonhuman primates, and mice. *PNAS*. 116:26173–26180.

Van Essen DC, Lewis JW, Drury HA, Hadjikhani N, Tootell RB, Bakircioglu M, Miller MI. 2001. Mapping visual cortex in monkeys and humans using surface-based atlases. *Vision Res*. 41:1359–1378.

Van Essen DC. 1997. A tension-based theory of morphogenesis and compact wiring in the central nervous system. *Nature*. 385:313–318.

Vanduffel W, Fize D, Mandeville JB, Nelissen K, Van Hecke P, Rosen BR, Tootell RB, Orban GA. 2001. Visual motion processing investigated using contrast agent-enhanced fMRI in awake behaving monkeys. *Neuron*. 32:565–577.

Weiner KS, Barnett MA, Witthoft N, Golarai G, Stigliani A, Kay KN, Gomez J, Natu VS, Amunts K, Zilles K, et al. 2018. Definingthe most probable location of the parahippocampal place area using cortex-based alignment and cross-validation. *Neuroimage*. 170:373–384.

Weiner KS, Golarai G, Caspers J, Chuapoco MR, Mohlberg H, Zilles K, Amunts K, Grill-Spector K. 2014. The mid-fusiform sulcus: a landmark identifying both cytoarchitectonic and functional divisions of human ventral temporal cortex. *Neuroimage*. 84:453–465.

Weiner KS, Grill-Spector K. 2010. Sparsely-distributed organization of face and limb activations in human ventral temporal cortex. *Neuroimage*. 52:1559–1573.

Weiner KS, Grill-Spector K. 2011. Not one extrastriate body area: using anatomical landmarks, hMT+, and visual field maps to parcellate limb-selective activations in human lateral occipitotemporal cortex. *Neuroimage*. 56:2183–2199.

Weiner KS, Grill-Spector K. 2015. The evolution of face processing networks. *Trends Cogn Sci*. 19:240–241.

Weiner KS. 2019. The mid-fusiform sulcus (sulcus sagittalis gyri fusiformis). *Anat Rec (Hoboken)*. 302:1491–1503.

Welker W. 1990. Why does cerebral cortex fissure and fold? A review of determinants of gyri and sulci. In: Peters A, Jones EG, editors. *Cerebral Cortex*. New York: Plenum, pp. 3–136.

Willenbockel V, Sadr J, Fiset D, Horne GO, Gosselin F, Tanaka JW. 2010. Controlling low-level image properties: the SHINE toolbox. *Behav Res Methods*. 42:671–684.

Witthoft N, Nguyen ML, Golarai G, LaRocque KF, Liberman A, Smith ME, Grill-Spector K. 2014. Where is human V4? Predicting the location of hV4 and VO1 from cortical folding. *Cereb Cortex*. 24:2401–2408.

Zilles K, Palomero-Gallagher N, Amunts K. 2013. Development of cortical folding during evolution and ontogeny. *Trends Neurosci*. 36:275–284.